LAWRENCE
LIVERMORE
NATIONAL
LABORATORY

UCRL-PROC-206126

Design and progress toward a multi-conjugate adaptive optics system for distributed aberration correction

K. Baker, S. Olivier, J. Tucker, D. Silva, D. Gavel, R. Lim, E. Gratrix

August 18, 2004

SPIE
Denver, CO, United States
August 2, 2004 through August 6, 2004

Design and progress toward a multi-conjugate adaptive optics system for distributed aberration correction

K.L. Baker, S.S. Olivier, J. Tucker, D.A. Silva, D. Gavel, R. Lim and E. Gratrix

Lawrence Livermore National Laboratory, Livermore, CA, USA

Abstract

This article investigates the use of a multi-conjugate adaptive optics system to improve the field-of-view for the system. The emphasis of this research is to develop techniques to improve the performance of optical systems with applications to horizontal imaging. The design and wave optics simulations of the proposed system are given. Preliminary results from the multi-conjugate adaptive optics system are also presented. The experimental system utilizes a liquid-crystal spatial light modulator and an interferometric wave-front sensor for correction and sensing of the phase aberrations, respectively.

keywords: Multi-Conjugate, Adaptive, Optics

I. INTRODUCTION

Turbulence is distributed along the direction of propagation of light passing through the atmosphere. Conventional adaptive optics systems use a single guide star to collect information regarding the line-integrated phase distortion from a single field angle. This limits the corrected field-of-view to a small isoplanatic patch around the guide star. Light coming from different field angles, however, travel through physically different regions in those turbulence layers that are removed from the entrance pupil of the system, as shown in Figure 1, and are therefore not well corrected with a single guide star. Multi-conjugate adaptive optics (MCAO) systems greatly reduce this limitation by collecting light from multiple guide stars at separate field angles. Through tomographic reconstruction of the resulting line-integrated phase distortion measurements from multiple field angles, the three dimensional turbulence profile can be determined. In addition, multiple deformable mirrors are placed at conjugate altitudes to the turbulence layers in the atmosphere such that the individual turbulence layers can be corrected thereby greatly enhancing the corrected field-of-view. Even without the use of multiple deformable mirrors, the tomographic reconstruction of the turbulence will be required to correct for focal anisoplanatism using laser guide stars in the next generation of extremely large telescopes.

II. CHARACTERIZATION OF THE LIQUID-CRYSTAL SPATIAL LIGHT MODULATOR

The approach taken to perform the initial characterization of the liquid-crystal spatial light modulator was to set up a Twyman-Green interferometer as the characterization instrument, as shown in Fig.2. A tilt is placed on the reference leg of the Twyman-Green interferometer such that a large number of fringes, ~100, are apparent in the interference pattern on the CCD camera. Fourier transforming the interference pattern produces a Fourier spectrum, which has a DC component and an up and down shifted satellite structure due to the large carrier frequency introduced by the applied tilt on the reference leg. By filtering all but the up-shifted satellite structure and shifting this structure back to the origin, the phase can be determined. The wrapped phase calculated in this manner is equal to the inverse tangent of the imaginary part divided by the real part of the inverse Fourier transform. The wrapped phase is then unwrapped using four separate unwrapping schemes.

The process has been automated and includes the steps described below. The first step is to register the spatial light modulator and remove any tilt between the liquid crystal spatial light modulator and the CCD camera in software. The initial registration and rotation adjustment are taken care of by writing three gaussians to three of the corners of the SLM. An image of the LC-SLM with and without the gaussians are taken, both with the reference leg blocked. The two images are subtracted from one another and a center-of-mass is used to locate the centers of the gaussians. The rotation is removed by rotating the image acquired from the camera such that the gaussian locations are along the appropriate row or column in which they were applied to the SLM. The registration process is repeated to verify that the rotation has been removed.

Once the rotation has been removed and the registration performed, then the next step is to uncover the reference arm such that the CCD camera is acquiring interferograms. The next step is to send a series of gaussians of varying amplitude to the spatial light modulator. For this process, the gaussians written to the spatial light modulator had a width of 75 pixels, $Amp*\exp(-(r/width)^2)$, and the amplitude varied from 0 to 255 in increments of 10. For each gaussian, a square of 50 by 50 pixels was used centered around the peak of the gaussian. By taking a 50x50 pixel region, approximately 81 gaussian(9 by 9) locations were written to the spatial light modulator to cover the 440 by 440 pixels characterized on the SLM. For each Gaussian location, 27 gaussians were written to the SLM with amplitudes ranging from 0 to 255 in increments of 10. Each interferogram recorded is processed to determine the wrapped phase, then the wrapped phase is unwrapped using several different unwrapping routines, the piston and tip/tilt are removed from the unwrapped phases over regions of the spatial light modulator for which no phase was applied and finally the phase with zero volts applied to the SLM is subtracted to take out the phase aberration of the unpowered SLM. Once the phase vs. amplitude has been determined, a fourth order polynomial is fit to the response for rapid application of the correction when running in closed-loop. This entire process takes approximately 10 hours to finish and is therefore started in the evening and is done by the next morning.

The next step is to test the phase vs. amplitude written to the SLM by running the spatial light modulator in closed loop to take out the residual phase aberration of the unpowered spatial light modulator. The initial phase aberration of the spatial light modulator is shown below in Fig. 3c. This process starts by

measuring the phase of the SLM, multiplying the measured phase by the gain, 0.9, and then applying the correction.. The integrator weight for this process was set to unity and the gain to 0.9. The measured variance as a function of iteration number is shown in Fig. 3a and the Strehl ratio, calculated from the Marechal approximation with the measured variance, is given in Fig. 3b. The initial correction sent to the spatial light modulator is shown in Fig. 3c and the residual phase after ten iterations is shown in Fig. 3d.

III. PHASE PLATE MANUFACTURE AND CHARACTERIZATION

To decrease the cost of manufacturing phase plates needed to characterize the multi-conjugate adaptive optics system, a process of phase plate replication via optical epoxy was undertaken. The optical epoxy replicas are made from an original phase screen that was etched in glass using a binary etching process described below. By making the phase plates from a sandwich of two different optical epoxies, the turbulence strength of the plates can be set by choosing the change in index of refraction of the two optical epoxies. The original phase screen was fabricated by the Microfabrication Laboratory at the Lawrence Livermore National Laboratory (LLNL) for the Laboratory for Adaptive Optics at the University of California at Santa Cruz. The process of manufacturing phase plates via binary glass etching has been used previously[1] and this particular process was developed at LLNL for the Coherent Communications Imaging and Targeting project.[2] The Laboratory for Adaptive Optics loaned the original phase plate for the purpose of investigating this technique of manufacturing the phase plates which is approximately an order of magnitude less expensive than the glass etching process. The process of glass etching is described in the next paragraphs followed by a description of the optical epoxy replication process and characterization work done on the replicated phase screens.

For the original phase screen, the Laboratory for Adaptive Optics chose a design consisting of 256 phase levels, which required eight binary masks ($2^8 = 256$ levels). The simulated Kolmogorov phase profile for the mask was decomposed into these 8 binary masks, each with the binary etch depths required for the given phase variation. The phase mask was manufactured on a 10 cm by 10 cm substrate of crown glass. Once the design was complete, the eight files, one for each mask, were sent to a lithography mask manufacturer to obtain the eight binary masks used to fabricate the phase screen. A fourteen step process was used to manufacture the phase plates and is listed in Table 1. The first step was to strip the photoresist from the glass plates, which came from the vendor with a layer of chrome. The next step was to strip the

Chrome and to clean the plates. At that point both sides of the plates were sputtered coated with 1000 Å chrome layers. The lithography component involved spinning a positive photoresist onto the surface and baking. The lithography masks were aligned with the substrate and exposed to ultraviolet radiation. The substrate was then developed and baked again. Next the substrate was descumed and the metal etched. The photoresist was stripped and the plates were cleaned. The metal thickness left on the plates was then measured, followed by etching the glass using buffered hydrofluoric acid. The metal thickness left on the plates was then measured again and the chrome layer was then stripped off. The final step in the process was to measure the etch depth in the glass. The process was then repeated starting at step two to achieve the required number of layers.

The process for replication of the phase screens was then performed. The replication process was undertaken by Vitrum Technology, LLC and is shown graphically in Fig. 4. The first step was to generate a master of the original phase plate. This required that the original glass phase plate by treated with a proprietary releasing process such that master material, Sylgard 184, did not stick to the glass phase screen. An adhesion promoter for Sylgard 184 was applied to a 10 by 10 cm sheet of glass. Sylgard 184 was placed on the glass master and degassed prior to placing the plate on top forming a sandwich. The silicone was cured for 48 hours and the master released from the sandwich. The epoxy replicas were then manufactured by applying a thin layer of optical epoxy to the master phase plate and a 10 cm by 10 cm glass plate on top. Ultraviolet light was used to cure the optical epoxy, which was then removed from the PDMS master plate. The "sandwich" phase plate was then made by applying a thin layer of the second epoxy onto the first epoxy layer. A glass plate is applied on top of the second epoxy layer and the second epoxy is cured with ultraviolet radiation.

The turbulence strength of a given plate combination can be changed using the same master slide but varying the difference in the indicies of refraction of the two optical epoxies. The phase structure function is defined by $D_\phi(r) = <|\phi(x) - \phi(x+r)|^2>$, which for a Kolmogorov turbulence spectrum can be expressed analytically as $D_\phi(r) = 6.88(r/r_o)^{5/3}$, in the limit $r>>(\lambda L)^{0.5}$. In this expression, r_o is the Fried parameter or transverse coherence length and λ and L are the wavelength and propagation length, respectively. Equating these two expressions the relationship between the Fried parameter and the difference in phase can be approximated as $|\phi(x)-\phi(x+r)| \alpha r_o^{-5/6}$ where the difference in phase is

proportional to the difference in the index of refraction of the two materials. The new value for the Fried parameter can then be expressed in terms of the old value and the differences in the indices of refraction or $r_{o\_new} = r_{o\_old}(\Delta n_{new}/ \Delta n_{old})^{-6/5}$.

The original glass etched phase plate was characterized by measuring the aberrated phase profile passing through the plate and subsequently unwrapping the phase. This task was accomplished by taking interferograms of the phase plate. The interferograms allowed the determination of the two-dimensional wrapped (modulo-2π) phase across the input aperture of the system. Before the Fried parameter used to describe the turbulence spectrum could be determined, the phase had to be unwrapped. The phase was unwrapped using a minimum weighted discontinuity method for the original glass phase plate.[3] This technique partitions the wrapped phase profile into two connected regions, separated by discontinuity curves. The algorithm then raises the phase in one of the regions by 2π thereby reducing the weighted sum of the discontinuities. This process is repeated until no further partitioning is possible. An example of a wrapped phase determined from a single set of sine and cosine interferograms is shown in Figure 5(a) below. After processing the wrapped phase with the minimum weighted discontinuity algorithm, the unwrapped phase shown in Figure 5(b) was recovered. The unwrapped phase consists primarily of tilt, as expected from a Kolmogorov turbulence spectrum, and varies over approximately 100 radians, or almost 16 waves. The phase structure function is constructed by comparing the phase at a given location to the phase at an increasing distance from that location. The results from a single frame are shown in Figure 5(c). In this figure the black line denotes the phase structure function determined from the experimentally measured phase across the aperture. The solid gray line denotes an analytic fit to the structure function assuming a Kolmogorov turbulence spectrum and a Fried parameter of 0.32 mm.

This characterization process was then repeated for the replicated phase plate. In this case the two epoxies had a relative difference in their index of refraction of 0.05. A quadrature interferometer was again used to determine the wrapped (modulo-2π) phase across the input aperture of the system as shown in Figure 6(a). For the replicated plates, a large tilt is introduced, presumably because the two glass plates are not parallel when the epoxy is cured. For these phase plates the wrapped phase was unwrapped using a multigrid least squares method[4] giving the unwrapped phase shown in Figure 6(b). For the replicated phase plates, the anomalous tilt introduced was removed and the short exposure structure function fit to the data,

$D_\phi(r) = 6.88(r/r_O)^{5/3}(1\text{-}r/D)^{1/3}$. The results from a single frame are shown in Figure 6(c). In this figure the black line denotes the phase structure function determined from the experimentally measured phase across the aperture. The solid gray line denotes an analytic fit to the structure function assuming a Kolmogorov turbulence spectrum and a Fried parameter of 2.2 mm.

IV. EXPERIMENTAL LAYOUT

The testbed, shown in Figure 7, currently consists of an interferometric wave-front sensor and a liquid-crystal spatial light modulator. The liquid-crystal spatial light modulator is partitioned into four separate quadrants with each quadrant representing a potential independent deformable mirror, as illustrated in Figure 8. A three pass design is utilized to turn the liquid-crystal spatial light modulator into effectively three separate spatial light modulators, each with up to 240 x 240 pixels. Lens multiplexing is used to relay image the phase planes in the appropriate order for scintillation compensation[5] and to position the images precisely on the spatial light modulator. The natural guide stars are produced using two crossed transmission gratings. This technique provides nine guide stars in a regular grid pattern. A subset of these nine guide stars can be selected by filtering in the Fourier plane to remove select guide stars or to change the relative amplitude of the guide stars. The angular separation between the guide stars can be varied by changing the magnification of the imaging telescope placed between the crossed transmission gratings and the entrance pupil of the system.

Polarization components are utilized in the testbed to form the two interferograms with a $\pi/2$ phase shift between them and also to control the relative signal levels in the arms of the interferometer. The laser passes through the crossed transmission gratings to generate the nine guide stars. These nine guide stars are then sent through a beamsplitter to generate the nine probe beams that will sample the phase screens at different field angles and also to create nine reference beams for the interferometer. The reference beams are relay imaged for 9.2 meters and passed through a quarter wave plate to produce circularly polarized light before they are then combined with the guide star probe beams. The probe beams pass through the three aberrating phase plates that were designed to simulate atmospheric turbulence with a

Kolmogorov turbulence spectrum. After traversing the phase plates, the probe beams pass though the pupil of the system, also the third phase plate layer, that is then relay imaged onto the upper left-hand quadrant of the liquid-crystal spatial light modulator. The probe beams then pass through another imaging telescope, which places the second phase plate layer onto the lower right-hand quadrant of the liquid-crystal spatial light modulator. A third imaging telescope is then used to place the first phase plate layer onto the lower left-hand quadrant of the liquid-crystal spatial light modulator. The probe beams are then sent through a half wave-plate to rotate their polarization by 45 degrees and combined with the reference beams. A relay imaging telescope reduces the pixel size of the spatial light modulator to match the CCD camera pixel size of the wave-front camera. A wollaston prism is then used to separate the sine and cosine interferograms onto the detector.

V. TOMOGRAPHIC RECONSTRUCTION USING ZERNIKE DECOMPOSITION

The approach taken for the three-dimensional reconstruction of the turbulence profile is to fit Zernike polynomials up to a specified order at each of the phase screens.[6] The geometry of the tomographic problem is illustrated in Fig. 9. This allows the tomography problem to be expressed as a system of algebraic equations for the unknown Zernike coefficients. By collecting line-integrated phase information from multiple guide stars, the appropriate coefficients for the Zernike polynomial series can be solved for and hence the phase at each layer determined. The resultant system of algebraic equations can be expressed in matrix form, B=HA where B is an array of optical path differences for each ray, H is the array of Zernike polynomial values for each ray coordinate at each of the phase screens and A is the array of Zernike coefficients describing the phase profile at each phase screen. To retrieve the Zernike coefficients of the phase, it is necessary to solve the algebraic system by inverting the array H. For the results presented below, A was solved by inverting the matrix H via singular value decomposition.

An example of the results obtained by this method are shown in Fig. 10. In this case three phase screens were used with a combined D/r_o of 10,where D is the diameter of the pupil and r_o is the Fried parameter. The phase input at each of the phase screens contained a Kolmogorov turbulence spectrum fit to the first 150 Zernike polynomials. Fig. 10a shows the applied phase at one of the phase screens and Fig. 10b shows the reconstructed phase. The residual phase variance of the nine guide stars passing through the three phase screens containing either the applied or reconstructed phases is shown in Fig. 10c. The

reconstruction used nine guide stars, 150 Zernike polynomials and 100 uniformly distributed phase points per guide star.

VI. INITIAL TESTBED RESULTS

The testbed, illustrated in Fig. 7 has been assembled with the liquid-crystal spatial light modulator and the pickoff mirrors to the point of demonstrating the concept of multiplexing the liquid-crystal spatial light modulator and using pickoff mirrors to successfully. It also demonstrates the generation of nine natural guide star beams using the crossed transmission gratings at the appropriate angular spacing with the imaging telescope. An example of the measured interferograms with a tilt placed on the reference beam is shown in Fig. 11. In this case the eighteen interferograms shown represent the nine natural guide star channels for both the sine and cosine channels.

The testbed design, illustrated in Fig. 7, was simulated with a wave optics code to verify its performance. This code is not yet integrated with the tomography code described above. In this case the turbulence is applied at the appropriate screen location and the inverse phase is applied at the conjugate plane representing the deformable mirror locations. This code Fresnel propagated the guide star beams through the MCAO testbed. In this simulation, the lenses, as well as the Kolmogorov turbulence, were treated as discrete phase screens. The simulation began with a uniform intensity profile at the crossed transmission gratings and then Fresnel propagated the amplitude and phase between the phase screens representing the lenses and the atmospheric turbulence. Fig. 12c shows the point spread function for the nine guide star beams arranged in a grid when there are no atmospheric turbulence screens placed in the system. When the phase screens are added to the system with a $d/r_o = 10$, then the point spread function degrades to that shown in Fig. 12a. Finally when the inverse phase is applied to the planes corresponding to the deformable mirror locations, then the point spread function shown in Fig. 12b results.

VII. SUMMARY

This article describes the progress towards a multi-conjugate adaptive optics system for increased field-of-view for a horizontal imaging system. A technique for characterizing liquid-crystal spatial light modulators was described utilizing a Twyman-Green interferometer. The response was then tested in closed-loop and found to achieve a Strehl ratio, in the Marechal approximation, of S_r=0.95. A phase plate

replication process was described as a way of significantly reducing the cost of manufacturing phase plates for testing of adaptive optics systems. The original phase plate was manufactured via acid etching of glass as describe above. The replication process was more than an order of magnitude cheaper, however, it did lead to increased amounts of tilt, likely due to insufficient parallelism between the sandwiched glass plates, and the high frequency response did not track the Kolmogorov structure function. The results are from the first master made and more masters will be made and the process refined. The design of a multi-conjugate adaptive optics system based on an interferometric quadrature detector was presented. A scheme for optical multiplexing such that a single liquid-crystal spatial light modulator could be used to effectively create four separate deformable mirrors with the turbulence layers imaged in the appropriate order to correct scintillation was also presented. Wave optics simulations of the design were carried out with the inverse phase applied at the appropriate deformable mirror planes and the design validated. The testbed was also constructed and a preliminary test of the natural guide star generation, optical multiplexing of the liquid-crystal spatial light modulator and interferometric wave-front sensor were carried out. In addition, a tomography code based on Zernike decomposition was written and shown to accurately reproduce the Kolmogorov phase screens.

Acknowledgements

This work was performed under the auspices of the U.S. Department of Energy by the University of California, Lawrence Livermore National Laboratory under contract No. W-7405-Eng-48.

REFERENCES

[1] K.W. Billman, J.A. Breakwell, R.B. Holmes et al., presented at the Airborne Laser Advanced Technology II, Orlando, Florida, 1999 (unpublished).

[2] K.L. Baker, E.A. Stappaerts, S.C. Wilks et al.,"Open and Closed-Loop Aberration Correction using a Quadrature Interferometric Wave-Front Sensor," Opt. Lett. **29** (1), 47 (2004); K.L. Baker, E.A. Stappaerts, D. Gavel et al.,"Breadboard Testing of a Phase Conjugate Engine with an Interferometric Wave-Front Sensor and a MEMS-Based Spatial Light Modulator," Appl. Opt (2004).

[3] Thomas J. Flynn,"Two-dimensional phase unwrapping with minimum weighted discontinuity," JOSA A **14** (10), 2692 (1997).

[4] Mark D. Pritt,"Phase Unwrapping by Means of Multigrid Techniques for Interferometric SAR," IEEE Transactions on Geoscience and Remote Sensing **34** (3), 728 (1996).

[5] Ralf C. Flicker,"Sequence of phase correction in multiconjugate adaptive optics," Opt. Lett. **26** (22), 1743 (2001).

[6] George N. Lawrence and Weng W. Chow,"Wave-front tomography by Zernike polynomial decomposition," Opt. Lett. **7** (9), 267 (1984).

FIGURE CAPTIONS

Figure 1 Illustration of the necessity of multi-conjugate adaptive optics (MCAO).

Figure 2 Twyman-Green interferometer used to characterize the liquid-crystal spatial light modulator.

Figure 3 Closed loop verification of the response of the liquid-crystal spatial light modulator. Fig 3a, 3b, 3c and 3d show the variance in the measured phase as a function of iteration number, the corresponding Strehl ratio in the Marechal approximation as a function of iteration number, the initial phase aberration attributed to the unpowered spatial light modulator and the residual phase after ten iterations, respectively.

Figure 4 Phase screen replication process steps to make optical epoxy replicas of the original glass etched phase plate.

Figure 5 Phase profile across the aperture of the probe beam passing through the original acid-etched glass phase plates. This particular phase profile was determined from a single set of sine and cosine interferograms. The wrapped and unwrapped phases and the resultant structure function are displayed in 5a, 5b and 5c, respectively.

Figure 6 Phase profile across the aperture of the probe beam passing through the replicated phase plate with $\Delta n=0.05$. This particular phase profile was determined from a single set of sine and cosine interferograms. The wrapped and unwrapped phases and the resultant short-exposure structure function are displayed in 6a, 6b and 6c, respectively.

Figure 7 Laboratory breadboard setup used to test the performance of the multi-conjugate adaptive optics system in a controlled laboratory environment. The abbreviations stand for the following: BS, beam splitters; M, mirrors; L, lenses; S, shutters; A, apertures; TFP, thin film polarizers; $\lambda/2$ and $\lambda/4$, half and quarter wave-plates, respectively.

Figure 8 Optical setup for reimaging the phase screens in the appropriate order and for partioning the liquid-crystal spatial light modulator into four separate deformable mirrors.

Figure 9 Sine and cosine interferograms for the nine guide stars with a tilt placed between the reference and guide star beams.

Figure 10 Wave optics simulations of the testbed performance. Figure 10a, 10b and 10c show the uncorrected point spread function with D/ro=10, the corrected point spread function with the inverse phase applied to the deformable mirror planes and the point spread function with no aberrations in the system, respectively.

Figure 11 Geometry for the tomographic reconstruction of the aberrated phase screens.

Figure 12 Results for the tomographic resonstruction via Zernike decomposition. Figure 12a, 12b and 12c show the applied phase at the second phase screen, the reconstructed phase and the residual phase variance of the nine guide stars passing through the three phase screens containing either the applied or reconstructed phases.

Table 1 Fourteen step process for manufacturing the glass etched phase screens.

FIGURES

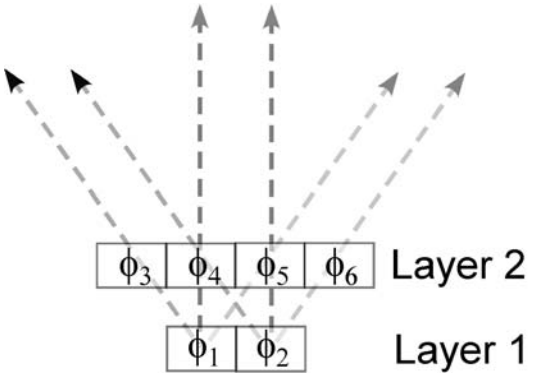

Figure 1

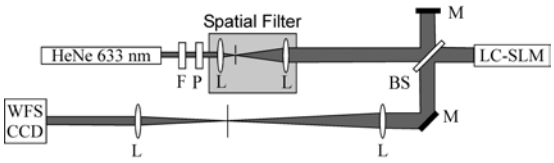

Figure 2

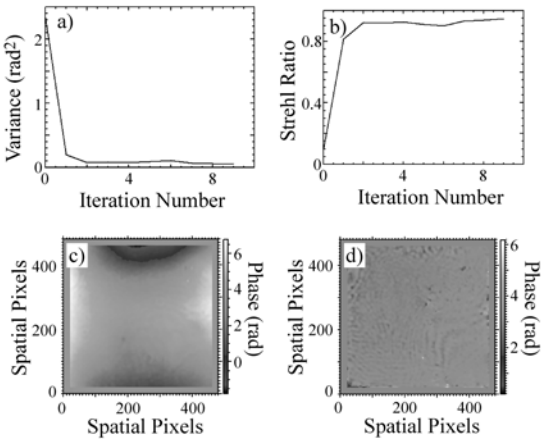
a)
Variance (rad²)
Iteration Number
b)
Strehl Ratio
Iteration Number
c)
Spatial Pixels
Spatial Pixels
Phase (rad)
d)
Spatial Pixels
Spatial Pixels
Phase (rad)

Figure 3

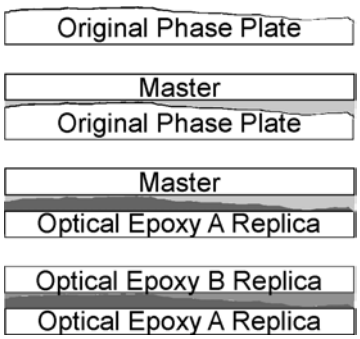
Original Phase Plate
Master
Original Phase Plate
Master
Optical Epoxy A Replica
Optical Epoxy B Replica
Optical Epoxy A Replica

Figure 4

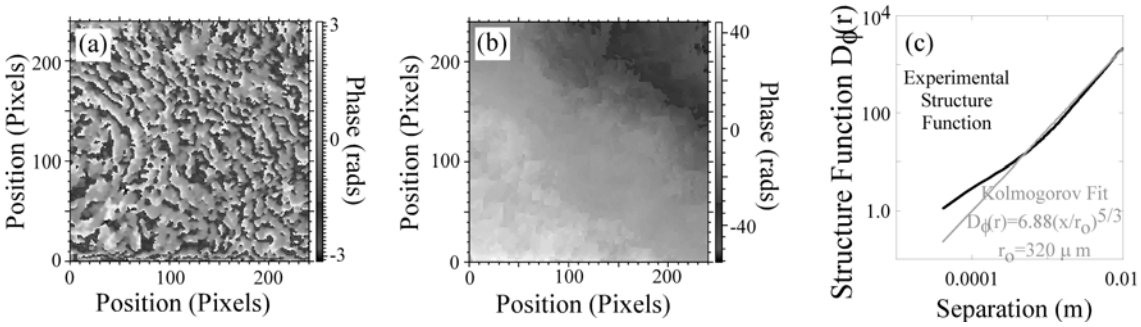
(a)
Position (Pixels)
Position (Pixels)
Phase (rads)
3
0
-3
(b)
Position (Pixels)
Position (Pixels)
Phase (rads)
40
0
-40
(c)
Experimental
Structure
Function
Kolmogorov Fit
$D_\phi(r)=6.88(x/r_o)^{5/3}$
r_o=320 μ m
Structure Function $D_\phi(r)$
Separation (m)
10^4
100
1.0
0.0001
0.01

Figure 5

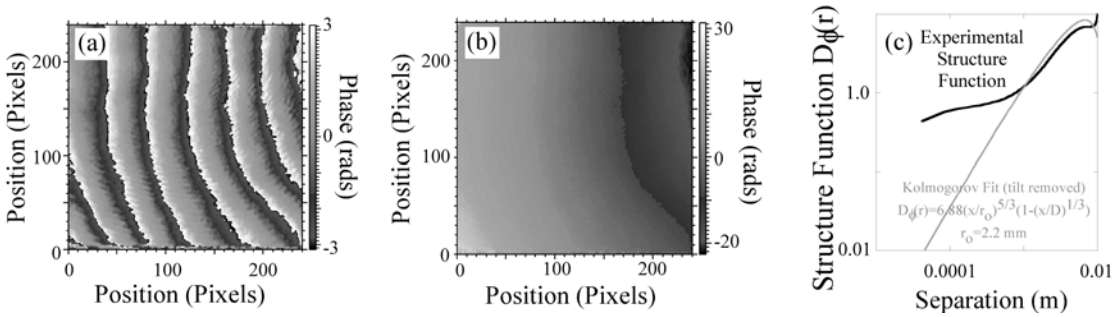
(a)
Position (Pixels)
Position (Pixels)
Phase (rads)
3
0
-3
0
100
200
(b)
Position (Pixels)
Position (Pixels)
Phase (rads)
30
0
-20
(c) Experimental Structure Function
Kolmogorov Fit (tilt removed)
$D_\phi(r)=6.88(x/r_o)^{5/3}(1-(x/D)^{1/3})$
r_o=2.2 mm
Structure Function $D_\phi(r)$
1.0
0.01
0.0001
0.01
Separation (m)

Figure 6

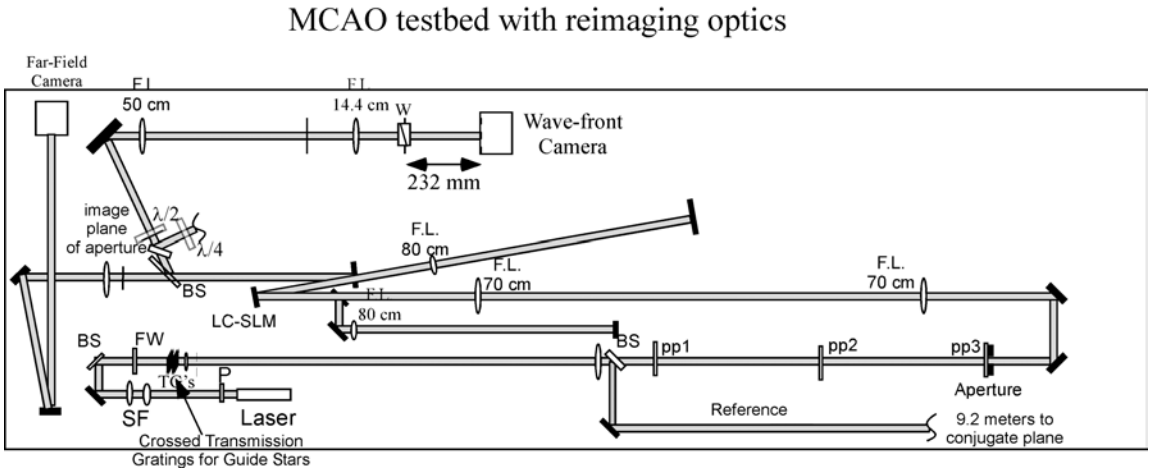
MCAO testbed with reimaging optics
Far-Field Camera
F.L. 50 cm
F.L. 14.4 cm
W
Wave-front Camera
232 mm
image plane of aperture
λ/2
λ/4
BS
F.L. 80 cm
F.L. 70 cm
F.L. 70 cm
LC-SLM
F.L. 80 cm
BS
FW
TGs
P
SF
Laser
Crossed Transmission Gratings for Guide Stars
BS
pp1
pp2
pp3
Aperture
Reference
9.2 meters to conjugate plane

Figure 7

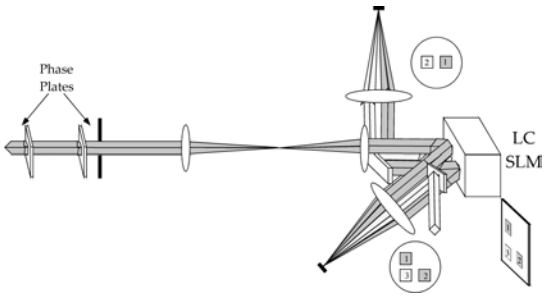

Figure 8

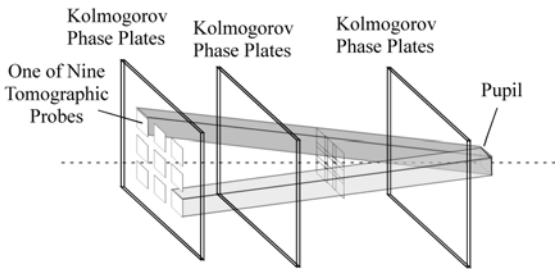
Kolmogorov
Phase Plates
Kolmogorov
Phase Plates
Kolmogorov
Phase Plates
One of Nine
Tomographic
Probes
Pupil

Figure 9

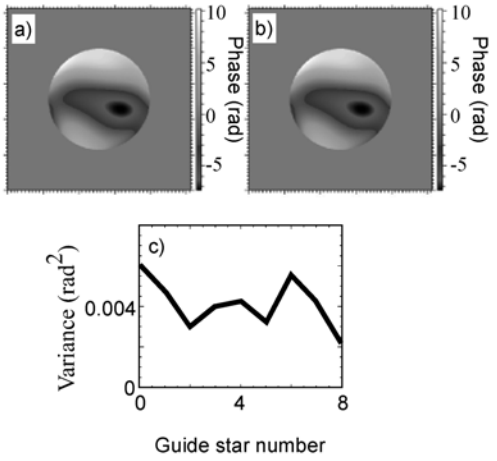
a)
b)
10
5
0
-5
Phase (rad)
c)
Variance (rad^2)
0.004
0
0
4
8
Guide star number

Figure 10

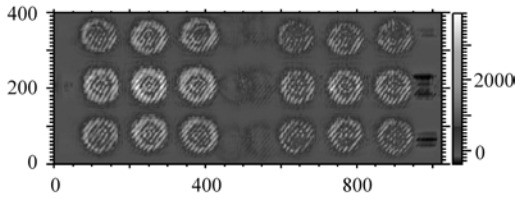

Figure 11

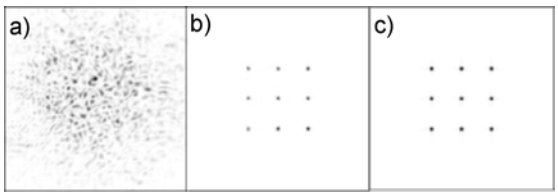

Figure 12

Step	Short Description
1	Strip photoresist
2	Strip Chrome
3	Clean
4	Chrome Sputter
5	Lithography
6	Descum
7	Metal Etch
8	Strip photoresist
9	Clean
10	Measure metal thickness
11	Glass Etch
12	Measure etch depth
13	Strip Chrome
14	Measure etch depth w/o chrome (verification)
	Repeat process (starting at step 2) as necessary to achieve required number of layers.

Table 1